The Astrophysical Journal, 720:872–886, 2010 September 1 doi:10.1088/0004-637X/720/1/872

A DETAILED SPECTROPOLARIMETRIC ANALYSIS OF THE PLANET-HOSTING STAR WASP-12*,†

L. Fossati[1], S. Bagnulo[2], A. Elmasli[1,7], C. A. Haswell[1], S. Holmes[1], O. Kochukhov[3], E. L. Shkolnik[4], D. V. Shulyak[5], D. Bohlender[6], B. Albayrak[7], C. Froning[8], and L. Hebb[9]
[1] Department of Physics and Astronomy, Open University, Walton Hall, Milton Keynes MK7 6AA, UK; l.fossati@open.ac.uk, elmasli@ankara.edu.tr, C.A.Haswell@open.ac.uk, s.holmes@open.ac.uk
[2] Armagh Observatory, College Hill, Armagh BT61 9DG, UK; sba@arm.ac.uk
[3] Department of Physics and Astronomy, Uppsala University, SE-751 20, Uppsala, Sweden; Oleg.Kochukhov@fysast.uu.se
[4] Department of Terrestrial Magnetism, Carnegie Institution of Washington, 5241 Broad Branch Road, NW, Washington, DC 20015, USA; shkolnik@dtm.ciw.edu
[5] Institute of Astrophysics, Georg-August-University, Friedrich-Hund-Platz 1, D-37077, Göttingen, Germany; denis.shulyak@gmail.com
[6] Herzberg Institute of Astrophysics, National Research Council of Canada, 5071 West Saanich Road, Victoria, BC V9E 2E7, Canada; david.bohlender@nrc-cnrc.gc.ca
[7] Department of Astronomy and Space Sciences, Ankara University, 06100, Tandoğan, Ankara, Turkey; balbayrak@ankara.edu.tr
[8] Center for Astrophysics and Space Astronomy, University of Colorado, 593 UCB, Boulder, CO 80309-0593, USA; cynthia.froning@colorado.edu
[9] Department of Physics and Astronomy, Vanderbilt University, 6301 Stevenson Center, Nashville, TN 37235, USA; leslie.hebb@vanderbilt.edu
Received 2010 June 11; accepted 2010 July 14; published 2010 August 13

ABSTRACT

The knowledge of accurate stellar parameters is paramount in several fields of stellar astrophysics, particularly in the study of extrasolar planets, where often the star is the only visible component and therefore used to infer the planet's fundamental parameters. Another important aspect of the analysis of planetary systems is the stellar activity and the possible star–planet interaction. Here, we present a self-consistent abundance analysis of the planet-hosting star WASP-12 and a high-precision search for a structured stellar magnetic field on the basis of spectropolarimetric observations obtained with the ESPaDOnS spectropolarimeter. Our results show that the star does not have a structured magnetic field, and that the obtained fundamental parameters are in good agreement with what was previously published. In addition, we derive improved constraints on the stellar age (1.0–2.65 Gyr), mass (1.23–1.49 $M/M_{\odot}$), and distance (295–465 pc). WASP-12 is an ideal object in which to look for pollution signatures in the stellar atmosphere. We analyze the WASP-12 abundances as a function of the condensation temperature and compare them with those published by several other authors on planet-hosting and non-planet-hosting stars. We find hints of atmospheric pollution in WASP-12's photosphere but are unable to reach firm conclusions with our present data. We conclude that a differential analysis based on WASP-12 twins will probably clarify whether an atmospheric pollution is present as well as the nature of this pollution and its implications in planet formation and evolution. We also attempt the direct detection of the circumstellar disk through infrared excess, but without success.

Key words: stars: abundances – stars: fundamental parameters – stars: individual (WASP-12) – stars: magnetic field

Online-only material: color figures, machine-readable table

1. INTRODUCTION

One of the biggest surprises in the exoplanet field was the discovery of gas giant planets orbiting very close to their host star. These hot Jupiter planets represent one extreme of the Galaxy's population of planets, and they provide important constraints to guide our nascent ideas about the formation and evolution of planetary systems. The probability of transit for close-in giant planets is ∼10% (Seager et al. 2000), and through the analysis of transit light curves the ratio of the stellar and planetary radii can be deduced. Through the significant uncertainties in the mass and radius of any particular star, our characterization of exoplanets is limited by that of their host stars (e.g., Southworth 2009). For this reason, it is important to directly measure the properties of planet-hosting stars, particularly in cases where we expect the presence of planets may have influenced the properties of the star through star–planet interactions.

One of the most extreme hot Jupiter exoplanets is WASP-12 b, a gas giant planet orbiting only 0.023 AU from a late F-type host star (Hebb et al. 2009). WASP-12 b's orbit is, therefore, only about 1.5 stellar diameters from the photosphere of the star. At such proximity, interactions between the star and the planet must occur. Near-UV observations of WASP-12 covering the wavelengths of many resonance lines reveal that WASP-12 b is surrounded by an exosphere which appears to overfill its Roche lobe (Fossati et al. 2010). This exospheric gas may be the consequence of tidal disruption of the planet's convective envelope as recently suggested by Li et al. (2010), but it could also be entrained material from the stellar corona.

A planet orbiting as close as WASP-12 b might be expected to interact magnetically with its host star (cf. Shkolnik et al. 2003; Shkolnik et al. 2005; Shkolnik et al. 2008). A first step to search for such interactions is to detect and quantify the stellar magnetic field by spectropolarimetry (e.g., Fares et al. 2010). The presence of a magnetic field belonging to WASP-12 would provide a precious piece of information needed to establish which mechanism controls the structure and the evolution of the disk (Lai et al. 2010).

* Based on observations obtained at the Canada-France-Hawaii Telescope (CFHT), which is operated by the National Research Council of Canada, the Institut National des Sciences de l'Univers of the Centre National de la Rechereche Scientifique of France, and the University of Hawaii.
† Based on observations made with the NASA/ESA *Hubble Space Telescope* obtained by MAST at the Space Telescope Science Institute, which is operated by the Association of Universities for Research in Astronomy, Inc., under NASA contract NAS 5-26555. These observations are associated with program 11651.

The solar system's giant planets have enhanced metal abundances relative to the Sun (Guillot 2005) and high atmospheric metal abundances have been suggested as a contributing factor in the inflated radii of planets such as WASP-12 b (Burrows et al. 2007). Intriguingly, Fossati et al. (2010) detected a wealth of metallic atoms and ions in the exospheric gas surrounding WASP-12 b. If this gas is indeed accreting onto the host star as suggested by Li et al. (2010), this could lead to abundance anomalies in the photosphere of WASP-12. Since WASP-12 is expected to have a very shallow surface convection zone, any accreted gas will remain close to the surface rendering any pollution of the surface composition relatively easy to detect.

In this paper, we report on spectropolarimetric observations of WASP-12 which we use to probe the stellar magnetic field, fundamental parameters, and abundance pattern of the star. In Section 2, we describe our observations and data reduction. Sections 3 and 4 provide a description of the adopted model atmosphere including methods and results of the stellar parameter determination and abundance analysis. In Section 5, we provide the results of our stellar magnetic field search. Our results are finally discussed in Section 6, while in Section 7 we gather our conclusions.

2. OBSERVATIONS AND DATA REDUCTION

We observed WASP-12 using the Echelle SpectroPolarimetric Device for ObservatioNs of Stars (ESPaDOnS) spectropolarimeter at the Canada–France–Hawaii Telescope (CFHT) on 2010 January 3 and 5. The observations were performed in "polarimetric" mode.

ESPaDOnS consists of a table-top cross-dispersed echelle spectrograph fed via a double optical fiber directly from a Cassegrain-mounted polarization analysis module. Beside the natural intensity, I, in polarimetric mode the instrument can acquire a Stokes V (or Q or U) profile throughout the spectral range 3700–10400 Å with a resolving power of about 65,000. A complete polarimetric observation consists of a sequence of four sub-exposures (Donati et al. 1997; Wade et al. 2000).

Each of the four sub-exposures was 1290 s long, with a total amount of integration time of 1.5 hr, each night. The spectra were reduced using the Libre-ESpRIT package[10] (Donati et al. 2007). The Stokes I spectra have a signal-to-noise ratio (S/N) per pixel of ∼126 and ∼158 in the continuum, on the first and second nights, respectively; both values calculated at 5000 Å. To increase the S/N of the Stokes I spectrum we averaged the two available spectra, obtaining a single spectrum with an S/N of ∼200, normalized by fitting a low order polynomial to carefully selected continuum points.

The effective temperature ($T_{\rm eff}$) was determined (see Section 4) from our ESPaDOnS data and two spectra of WASP-12 obtained at the Isaac Newton Telescope with the Intermediate Dispersion Spectrograph (IDS). The spectra cover the region of the Hα line with a spectral resolution of $R = 8000$ (see Hebb et al. 2009, for more details).

We also used near-UV observations obtained with the *Hubble Space Telescope* (*HST*) Cosmic Origin Spectrograph (COS; Green et al. 2010; Osterman et al. 2010) for the analysis of the spectral energy distribution. The spectra, calibrated in flux, cover three non-contiguous wavelength ranges in the near-UV with a resolution of $R \sim 20{,}000$. These observations are described in detail in Fossati et al. (2010).

[10] http://www.ast.obs-mip.fr/projets/espadons/espadons.html

3. THE MODEL ATMOSPHERE

To compute model atmospheres of WASP-12, we employed the LLmodels stellar model atmosphere code (Shulyak et al. 2004). For all the calculations LTE and plane-parallel geometry were assumed. We used the VALD database (Piskunov et al. 1995; Kupka et al. 1999; Ryabchikova et al. 1999) as a source of atomic line parameters for opacity calculations. The recent VALD compilation contains information for about 6.6×10^7 atomic transitions, most of them coming from the latest theoretical calculations performed by R. Kurucz.[11] Convection was implemented according to the Canuto & Mazzitelli (1991, 1992) model of convection (see Heiter et al. 2002, for more details).

4. FUNDAMENTAL PARAMETERS AND ABUNDANCE ANALYSIS

Hebb et al. (2009) derived the fundamental parameters of WASP-12 from the analysis of low and mid-resolution spectra, obtaining $T_{\rm eff} = 6300 \pm 150$ K, $\log g = 4.38 \pm 0.10$, and adopting a value of 0.85 km s^{-1} for the microturbulence velocity ($\upsilon_{\rm mic}$). We used these values as our starting point in an iterative process to gradually improve the parameters using different spectroscopic indicators. In our analysis, every time any of $T_{\rm eff}$, $\log g$, $\upsilon_{\rm mic}$ or abundances changed during the iteration process, we recalculated a new model with the implementation of the last measured quantities. Similarly the derived abundances were treated iteratively: while the results of the abundance analysis depend upon the assumed model atmosphere, the atmospheric temperature–pressure structure itself depends upon the adopted abundances, so we recalculated the model atmosphere every time abundances were changed, even if the other model parameters were fixed. This ensures the model structure is consistent with the assumed abundances.

We determined $T_{\rm eff}$ by fitting synthetic line profiles, calculated with SYNTH3 (Kochukhov 2007), to the observed profiles of two hydrogen lines: Hα (from the IDS spectrograph) and Hγ (from the ESPaDOnS spectropolarimeter). We discarded the other hydrogen lines observed with ESPaDOnS because of the uncertainties in the continuum normalization. In the temperature range expected for WASP-12, hydrogen lines are extremely sensitive to temperature variations and insensitive to $\log g$ variations and are therefore good temperature indicators. We found $T_{\rm eff} = 6250 \pm 100$ K, in good agreement with Hebb et al. (2009). The uncertainty estimate considered both the quality of the observations and the uncertainties in the normalization. Figure 1 shows the comparison between the observed Hα line profile and the synthetic profiles calculated with the adopted $T_{\rm eff}$ of 6250 ± 100 K. The poor fit of the hydrogen line core is due to the adopted LTE approximation (see, e.g., Mashonkina et al. 2009).

Another spectroscopic indicator for $T_{\rm eff}$ is given by the analysis of metallic lines that we performed on the ESPaDOnS spectrum. In particular, $T_{\rm eff}$ is determined by eliminating the correlation between abundance and excitation potential ($\chi_{\rm excit}$) for the selected lines of a given ion/element. The top panel of Figure 2 shows the correlation between abundance and $\chi_{\rm excit}$ for all measured lines of Ca I, Ca II, Fe I, Fe II, and Ni I. Figure 2, produced using the final adopted fundamental parameters, shows no significant correlation between abundance and $\chi_{\rm excit}$ for all ions, except Fe I, for which we registered a

[11] http://kurucz.harvard.edu

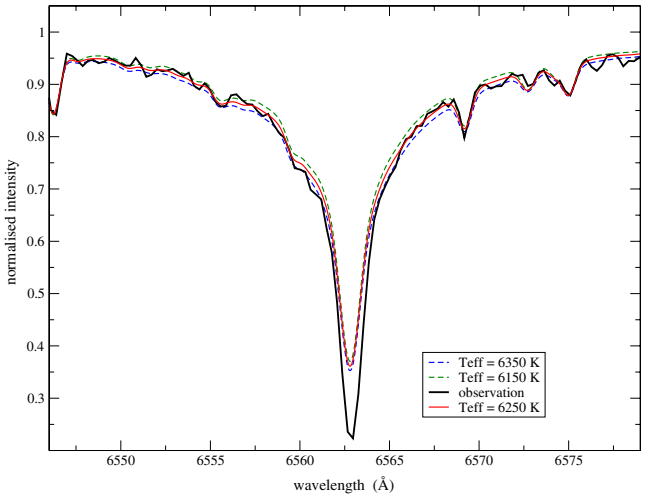

Figure 1. Comparison between the Hα line profile observed with the IDS spectrograph (black solid line) and synthetic profiles calculated with the final adopted $T_{\rm eff}$ of 6250 K (red solid line), and uncertainty (dashed lines).

(A color version of this figure is available in the online journal.)

slightly positive correlation (0.02263 ± 0.01139), that would be eliminated by a higher $T_{\rm eff}$. What we found here for Fe I resembles what remarked by Ryabchikova et al. (2009) for HD 49933 and HD 32115 (both stars have a $T_{\rm eff}$ slightly higher than WASP-12): an effective temperature determination based only on the analysis of Fe I lines leads systematically to a $T_{\rm eff}$ that is substantially higher (by about 5%), compared to the one obtained with other ions and in particular with other temperature indicators, such as hydrogen lines.[12] For this reason, we decided to use the analysis of the metallic lines only as consistency check of $T_{\rm eff}$ derived from the hydrogen lines. In addition to the ions shown in Figure 2, we also included in the consistency check C I, Si I, Sc II, Ti I, Ti II, V I, Cr I, Cr II, Mn I, Co I, and Y II, obtaining the requested equilibrium for all of them. The number of lines adopted to measure the abundance–$\chi_{\rm excit}$ correlation for each ion is the same as the one we used to derive the final ion abundance, and it is listed in Table 2.

The surface gravity was derived from two independent methods based on (1) line profile fitting of gravity-sensitive metal lines with developed wings and (2) ionization balance for several elements. The first method is described in Fuhrmann et al. (1997) and uses the fact that the wings of the Mg I lines at 5167, 5172, and 5183 Å are very sensitive to $\log g$ variations. In practice, we first derived the Mg abundance from other Mg I lines without developed wings, such as 5711 and 5785 Å, and then we fit the wings of the gravity indicator lines by tuning the $\log g$ value. To apply this method, very accurate $\log gf$ values and Van der Waals ($\log \gamma_{\rm Waals}$) damping constants are required for all the lines. We adopted the set of line parameters used by Ryabchikova et al. (2009) and included the uncertainty in these parameters in the uncertainty in $\log g$. We obtained a $\log g$ value of 4.2 ± 0.2, in good agreement with Hebb et al. (2009). Our line profile fit of the Mg I lines with developed wings is shown in Figure 3.

The second method, the ionization equilibrium, is often used to derive the surface gravity, but this method is extremely sensitive to the non-LTE effects present for each ion/element, while Mg lines with developed wings (less sensitive to non-LTE effects) are more suitable as $\log g$ indicators (Zhao & Gehren 2000). For this reason, we decided to keep the Mg lines as our primary $\log g$ indicator, and checked the result with the ionization equilibrium. Adopting the $\log g$ value obtained from the analysis of the Mg I lines with developed wings and taking into account the abundance uncertainties, we satisfied the ionization equilibrium for every element with two analyzed ions.

[12] We do not know the precise origin of this phenomenon and also whether it is present in a large temperature range or just for F-type stars. We believe that more work should be done in this respect, in particular because the $T_{\rm eff}$ determination based on the abundance–$\chi_{\rm excit}$ equilibrium is widely used to determine the effective temperature of stars in a broad $T_{\rm eff}$ range.

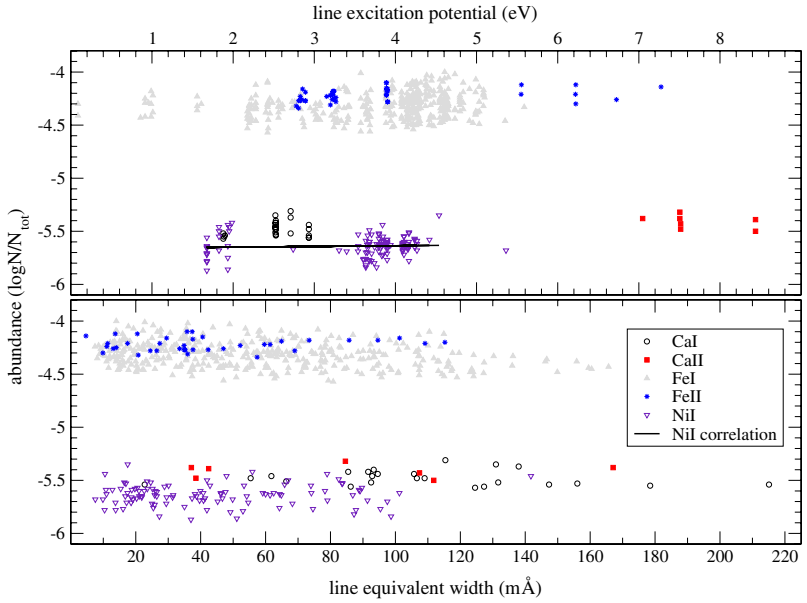

Figure 2. Top panel: abundance obtained for each measured line of Ca I (open circles), Ca II (filled squares), Fe I (filled triangles), Fe II (stars), and Ni I (open downside triangles) as a function of the line $\chi_{\rm excit}$. The black full line shows, as an example, the abundance-$\chi_{\rm excit}$ correlation for Ni I: 0.00637 ± 0.01270, consistent with zero. Bottom panel: abundance obtained for each measured line of the ions given in the top panel, as a function of the measured line equivalent width. The effective temperature from metallic lines is derived eliminating the correlation shown in the top panel, while $\upsilon_{\rm mic}$ is determined eliminating the correlation shown in the bottom panel.

(A color version of this figure is available in the online journal.)

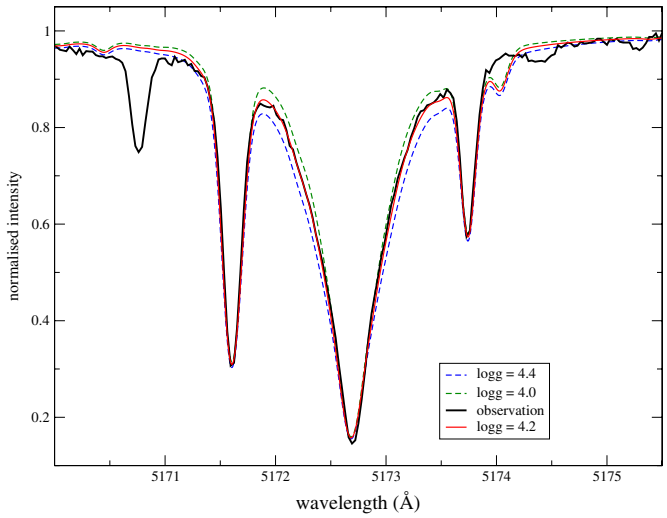

Figure 3. Comparison between the observed profile of the 5172 Å Mg I line (black solid line) and synthetic profiles calculated with the final adopted surface gravity of $\log g = 4.2 \pm 0.2$. We adopted the same combination of $\log gf$ and Van der Waals damping constants as in Ryabchikova et al. (2009): oscillator strengths from Aldenius et al. (2007) and damping constants from Fuhrmann et al. (1997).

(A color version of this figure is available in the online journal.)

Table 1
Line List of the Lines Used for the Abundance Analysis

Ion Wavelength (Å)	$\chi_{\rm excit}$ (eV)	$\log gf$	EQW (mÅ)	Abundance (dex)	Ref. $\log gf$
Li I					
6707.7610*	0.000	−0.009	S	−9.47	SLN
C I					
5023.8389	7.946	−2.209	12.14	−3.49	WFD
5800.6016	7.946	−2.338	9.51	−3.43	WFD
6014.8300	8.643	−1.585	15.74	−3.40	WFD
6671.8450	8.851	−1.651	9.97	−3.36	WFD
7111.4694	8.640	−1.086	26.93	−3.55	WFD
7116.9879	8.647	−0.907	36.47	−3.52	WFD
...	...	...	...	...	...

Notes. The first and second columns list, respectively, the $\chi_{\rm excit}$ (in eV) and the $\log gf$ value for each line. Columns 5 and 6 list the equivalent width in mÅ and the abundance for each line, while the last column gives the reference for the log gf value. Spectral lines for which the abundance were measured with synthetic spectra, instead of equivalent widths, present an "S" instead of the equivalent width value. Lines marked with "*" are subject to hyperfine structure, discussed in detail in the main text, while lines marked with "#" are multiplets (doublets or triplets) and in these cases we listed only the strongest line. SLN: Smith et al. (1998); WFD: Wiese et al. (1996).

(This table is available in its entirety in a machine-readable form in the online journal. A portion is shown here for guidance regarding its form and content.)

Our main source for the atomic parameters of spectral lines is the VALD database with the default configuration. LTE abundance analysis was based on equivalent widths, analyzed with a modified version (Tsymbal 1996) of the WIDTH9 code (Kurucz 1993a). For all analyzed elements/ions, we used almost all unblended spectral lines with accurate atomic parameters available in the wavelength range 4240–9900 Å, except lines in spectral regions where the continuum normalization was too uncertain. For blended lines, lines subjected to hyperfine splitting (hfs), lines situated in the wings of the hydrogen lines or for very shallow lines of specific ions we derived the line abundance by performing synthetic spectrum calculations with the SYNTH3 code. The hfs constants for abundance calculations were taken from Lawler et al. (2001b) for Eu II lines and from Smith et al. (1998) for the Li I line at 6707 Å. For the barium abundance, we used the Ba II lines at 5853.7 Å and 6496.9 Å for which we do not expect any relevant hfs effect (Mashonkina & Zhao 2006). A line-by-line abundance list with the equivalent width measurements, adopted oscillator strengths, and their sources are given in Table 1.

The microturbulence velocity was determined by minimizing the correlation between equivalent width and abundance for several ions, as shown in Figure 2 for Ca I, Ca II, Fe I, Fe II, and Ni I. To employ this method, we used all ions for which the measured spectral lines covered a large range in equivalent width. In particular, we took into account simultaneously: Si I, Ti I, Ti II, Cr I, Cr II, Mn I, and Y II, in addition to the ones present in Figure 2. The final adopted $\upsilon_{\rm mic}$ is 1.2 ± 0.3 km s^{-1}. The given error bar is the range of values resulting from minimization of the correlation for each ion we considered.

The projected rotational velocity and macroturbulence ($\upsilon_{\rm macro}$) were determined by fitting synthetic spectra of several carefully selected lines to the observed spectrum. Given the $\upsilon \sin i$–$\upsilon_{\rm macro}$ degeneracy, we followed Valenti & Fisher (2005): we measured $\upsilon_{\rm macro}$ assuming $\upsilon \sin i = 0$ km s^{-1} and then $\upsilon \sin i$ assuming $\upsilon_{\rm macro} = 4.75$ km s^{-1} (from the $T_{\rm eff}$–$\upsilon_{\rm macro}$ relation published by Valenti & Fisher 2005). In the first case, we obtained $\upsilon_{\rm macro} = 7.0 \pm 0.6$ km s^{-1}, while in the second case we obtained $\upsilon \sin i = 4.6 \pm 0.5$ km s^{-1}. In conclusion, $\upsilon \sin i$ is in the range 0–4.6 ± 0.5 km s^{-1}, while $\upsilon_{\rm macro}$ lies between 4.75 and 7.0 ± 0.6 km s^{-1}. It will be possible to precisely measure $\upsilon \sin i$ only with a careful analysis of the Rossiter–McLaughlin (RM) effect.

The final WASP-12 abundances, in $\log(N/N_{\rm tot})$, are given in Table 2 and the atmospheric abundance pattern is shown in Figure 4 in comparison to the solar abundances (Asplund et al. 2005). While the large overabundance of K would disappear if non-LTE effects are taken into account (Takeda et al. 1996), the Sr overabundance is genuine since non-LTE effects are expected to be less then 0.05 dex for the Sr lines we analyzed (Mashonkina et al. 2007, and references therein). In general, we expect small non-LTE effects for WASP-12 due to the high stellar metallicity.

The stellar metallicity (Z) is defined as follows:

$$Z_{\rm star} = \frac{\sum_{a \geqslant 3} m_a 10^{\log(N_a/N_{\rm tot})}}{\sum_{a \geqslant 1} m_a 10^{\log(N_a/N_{\rm tot})}}, \quad (1)$$

where a is the atomic number of an element with atomic mass $m_{\rm a}$. Our abundances imply a metallicity of $Z = 0.021 \pm 0.002$ dex, adopting the solar abundances by Asplund et al. (2005) for all the elements that we did not analyze.

The Z value adopted to characterize isochrones is calculated with the following approximation:

$$Z_{\rm star} \simeq 10^{([{\rm Fe/H}]_{\rm star} - [{\rm Fe/H}]_{\odot})} \cdot Z_{\odot}, \quad (2)$$

assuming $Z_{\odot} = 0.019$ dex. We recalculated the Z of WASP-12 according to this approximation obtaining $Z = 0.036 \pm 0.002$ dex.

Table 2
LTE Atmospheric Abundances of WASP-12 with Error Bar Estimates Based on the Internal Scatter from the Number of Analyzed Lines, n

Ion	WASP-12			Sun
	$\log(N/N_{\rm tot})$	n	$[N_{\rm el}/N_{\rm tot}]$	$\log(N/N_{\rm tot})$
Li I #	-9.47 ± 0.05	2	+1.52	−10.99
C I	-3.45 ± 0.08	14	+0.20	−3.65
N I #	−3.95	1	+0.31	−4.26
O I	−3.10	1	+0.28	−3.38
Na I	-5.63 ± 0.04	4	+0.24	−5.87
Mg I	-4.30 ± 0.13	4	+0.21	−4.51
Mg II	-4.29 ± 0.05	3	+0.22	−4.51
Al I	-5.63 ± 0.08	4	+0.04	−5.67
Si I	-4.47 ± 0.18	60	+0.06	−4.53
Si II	-4.33 ± 0.01	2	+0.20	−4.53
S I #	-4.78 ± 0.05	8	+0.12	−4.90
K I	−6.12	1	+0.84	−6.96
Ca I	-5.48 ± 0.07	24	+0.25	−5.73
Ca II	-5.41 ± 0.06	7	+0.32	−5.73
Sc II	-8.55 ± 0.07	8	+0.44	−8.99
Ti I	-6.95 ± 0.09	37	+0.19	−7.14
Ti II	-6.76 ± 0.09	24	+0.38	−7.14
V I	-7.99 ± 0.07	11	+0.05	−8.04
V II	-7.86 ± 0.03	2	+0.18	−8.04
Cr I	-6.17 ± 0.06	32	+0.23	−6.40
Cr II	-5.94 ± 0.06	12	+0.46	−6.40
Mn I	-6.41 ± 0.16	16	+0.24	−6.65
Fe I	-4.31 ± 0.12	389	+0.28	−4.59
Fe II	-4.22 ± 0.06	38	+0.37	−4.59
Co I	-6.98 ± 0.07	12	+0.14	−7.12
Ni I	-5.64 ± 0.10	105	+0.17	−5.81
Cu I	-7.81 ± 0.09	4	+0.02	−7.83
Zn I	−7.32	1	+0.12	−7.44
Sr I #	−8.30	1	+0.82	−9.12
Sr II#	-8.35 ± 0.05	3	+0.77	−9.12
Y II	-9.55 ± 0.09	10	+0.28	−9.83
Zr II	−9.08	1	+0.37	−9.45
Ba II	-9.37 ± 0.06	2	+0.50	−9.87
La II	−10.40	1	+0.51	−10.91
Ce II	-10.29 ± 0.07	3	+0.17	−10.46
Nd II	-10.45 ± 0.03	4	+0.14	−10.59
Sm II	−10.64	1	+0.39	−11.03
Eu II#	−11.30	1	+0.22	−11.52
Gd II#	$\leqslant -10.92$	1	+0.00	−10.92
$T_{\rm eff}$		6250 K		5777 K
$\log g$		4.20		4.44

Notes. The fourth column gives the WASP-12 abundances in dex relative to the solar values from Asplund et al. (2005). The last column gives the abundances of the solar atmosphere from Asplund et al. (2005). The lithium and europium abundances take hyperfine structure in the lines into account. The Gd II abundance is an upper limit. The symbol # indicates the ions for which the abundance was derived from line profile fitting, instead of equivalent widths.

4.1. Abundance Uncertainties

The abundance uncertainties for each ion, shown in Table 2, are the standard deviations of the mean abundance obtained from the individual line abundances. Following Fossati et al. (2009), it is possible to conclude that in case of ions with a sufficiently high number of lines, the internal scatter for each ion includes the uncertainties due to equivalent width measurement and continuum normalization. In addition, from plotting the abundance scatter as a function of the number of lines, we can also infer an internal uncertainty of 0.08 dex, that can be applied as mean scatter when only one line of a certain ion is measured.

Table 3 shows the variation in abundance for each analyzed ion, caused by the change of one fundamental parameter by $+1\sigma$, keeping fixed the other parameters.

Table 3 shows that the main source of uncertainty varies according to the element/ion (e.g., for the Fe-peak elements, neutrals are more sensitive to temperature variations, while ions are more sensitive to $\log g$ variations) and in some cases to the selected lines (e.g., the two Ba II lines selected to measure the Ba abundance are rather strong, therefore the Ba abundance is strongly dependent on $\upsilon_{\rm mic}$ variations).

Assuming the different uncertainties in the abundance determination are independent (though actually the systematic uncertainties will be correlated), we derived a pessimistic final error bar using standard error propagation theory, given in Columns 7 and 8 of Table 3. Using the propagation theory, we considered the situation where the determination of each fundamental parameter is an independent process. The mean value of the LTE uncertainties given in Column 8 of Table 3 is 0.11 dex. Due to the fact that for the parameter determination of both $T_{\rm eff}$, $\log g$ and $\upsilon_{\rm mic}$ we took into account all possible systematics (except non-LTE), we believe that the abundance uncertainties given in the last column of Table 3 can be considered as upper limits and that the real error bars lie between the values given in Columns 3 and 8 of Table 3.

5. HIGH PRECISION MAGNETIC FIELD SEARCH

One of the main goals of our analysis is to search for a global stellar magnetic field in WASP-12. The ESPaDOnS spectropolarimeter yields high resolution and high S/N spectra of both Stokes I and V allowing this search. To detect the presence of a global magnetic field and measure its strength we used the least-squares deconvolution technique (hereafter LSD), adopting a code written by one of us (O. Kochukhov).

LSD is a cross-correlation technique developed for the detection and measurement of weak polarization signatures in stellar spectral lines. The method is described in detail by Donati et al. (1997) and Wade et al. (2000). We decided to use the LSD approach to detect a magnetic field in WASP-12 since this method is the most precise currently available, especially for stars with rich line spectra and low projected rotational velocity ($\upsilon \sin i$), such as WASP-12.

We applied the LSD technique to the Stokes V spectra from each of the two nights using about 6450 atomic spectral lines with the only cutoff criterion based on the calculated line depth (>10%), and in both cases no magnetic field was found. From the spectrum of January 3rd we obtained $\langle B_z \rangle = 2.3 \pm 5.3$ G, with an S/N of the Stokes V LSD profile of 2400, while from the second night spectrum we obtained $\langle B_z \rangle = -10.1 \pm 4.2$ G, with an S/N of the Stokes V LSD profile of 3380. We obtained similar values also from both null profiles. Figure 5 shows the LSD profiles.

In late-type stars, the stellar magnetic field is directly connected to the chromospheric activity, that can be monitored with the Ca II H and Ks. In Figure 6, we compare the profiles of the Ca II H and K lines, observed with ESPaDOnS, with the mean line profiles of τ Boo (Shkolnik et al. 2005) obtained averaging several CFHT spectra acquired with the GECKO spectrograph.[13] This comparison is particularly valuable because both stars are planet-hosting and have similar fundamental parameters and age (Gonzalez et al. 2010a), where the difference is mainly in the $\upsilon \sin i$ values (τ Boo has a $\upsilon \sin i$ of

[13] http://www.cfht.hawaii.edu/Instruments/Spectroscopy/Gecko/

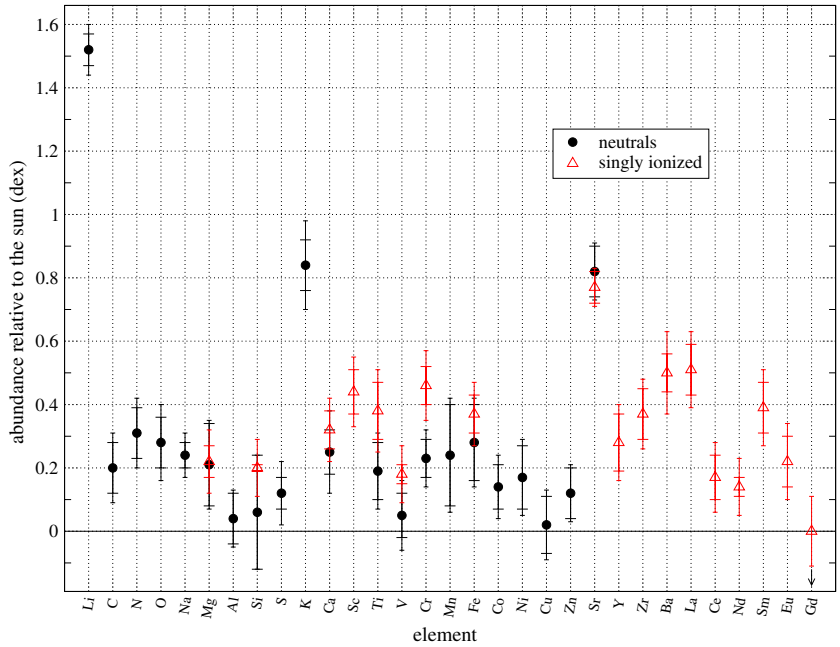

Figure 4. Ion abundance relative to the Sun (Asplund et al. 2005) of the WASP-12 atmosphere. Full points show the abundance of the neutral elements, while the open triangles show the abundance of the singly ionized elements. Each abundance value is shown with two uncertainty values: the standard deviation from the mean (Column 3 of Table 3) and the total uncertainty (Column 8 of Table 3). We believe the real uncertainty lies between these two values.

(A color version of this figure is available in the online journal.)

about 13.5 km s^{-1}). Figure 6 does not show the presence of any anomaly in WASP-12 Ca II H and K line cores. Knutson et al. (2010) determined the $\log(R'_{\rm HK})$ chromospheric stellar activity parameter in a set of planet-hosting stars, reporting for WASP-12 the remarkably low value of −5.500, the lowest in their sample.

The bottom panel of Figure 1 in Fossati et al. (2010) shows the core of the Mg II UV resonance lines (further stellar activity indicators) of WASP-12 and here the lack of any line core emission is clear, in agreement with the low level of stellar activity reported by Knutson et al. (2010).

It is well known that the chromospheric activity is strongly correlated with the stellar rotational velocity that for WASP-12 is unknown. Given the very small RM effect shown by Husnoo et al. (2010), it is probable that the low stellar activity of WASP-12 might be connected to a low rotational velocity. It is also possible that the star is either passing through a period of low activity, or WASP-12 is much older than reported by Hebb et al. (2009) (more than 1 Gyr older), or the typical signs of stellar activity, such as emission in the cores of the Mg II resonance lines, are absorbed by the material lost by the planet and falling onto the star (see Li et al. 2010; Fossati et al. 2010). A more thorough analysis and discussion of the stellar activity and of the reasons behind its low level will be given in a following work, now in preparation.

6. DISCUSSION

6.1. Atmospheric Parameters and Convection

Because WASP-12 has a relatively low effective temperature, its hydrogen lines are ideal indicators of atmospheric T–P structure. Generally, fitting hydrogen line profiles, rather than any other atomic line, provide an accurate estimate of $T_{\rm eff}$. On the other hand, at low temperatures, convection becomes an important energy transfer mechanism, influencing the photospheric temperature stratification and, thus, hydrogen line formation. The derived value of $T_{\rm eff}$ then depends on the convection treatment used in the model atmosphere calculations.

There are basically two formalisms of convection treatment available for model atmosphere computations: the well known mixing-length theory (MLT; Böhm-Vitense 1958), which relies on some free parameter (α), describing the characteristic length traveled by convective cells before they disappear, and further improvement of stellar convection developed by Canuto & Mazzitelli (1991, CM hereafter). The main advantage of the new model is that it does not require any adjustable parameters like α, which is now computed based on the geometrical depth scale inside the convective zone. It also accounts for the full spectrum of turbulent eddies and is therefore superior to the single-eddy assumption made by MLT. More details can be found in Canuto & Mazzitelli (1992).

Physically, the CM convection model is somewhat superior to MLT, therefore we preferred CM convection over MLT in our analysis. In the case of WASP-12, we find no critical differences in Hα profiles using both CM and MLT convection theories with the commonly accepted $\alpha = 1.25$. This is because the wings of Hα are formed mainly in the region right above the photosphere where convection plays a less important role in the energy balance. However, bluer Balmer lines are formed deeper and thus can show the changes in the temperature stratification introduced by convection. For instance, this is the case for the Hγ line for which MLT predicts weaker line wings (i.e., stronger convective energy transport): one needs an approximately 100 K hotter model to fit the Hγ line wings with MLT convection. However, it is then clear that only CM allows a consistent fit simultaneously for Hα and Hγ lines with the same $T_{\rm eff}$.

6.2. The Distance and Age of WASP-12

The basic parameters of WASP-12 were derived by Hebb et al. (2009). $T_{\rm eff}$, $\log g$, metallicity, and $\upsilon \sin i$ were derived from the observed stellar spectrum using spectral synthesis;

Table 3
Uncertainty Sources for the Abundances of WASP-12

Ion	Abundance $\log(N/N_{\rm tot})$	$\sigma_{\rm abn}$ (Scatt.) (dex)	$\sigma_{\rm abn}$ ($T_{\rm eff}$) (dex)	$\sigma_{\rm abn}$ ($\log g$) (dex)	$\sigma_{\rm abn}$ ($\upsilon_{\rm mic}$) (dex)	$\sigma_{\rm abn}$ (Syst.) (dex)	$\sigma_{\rm abn}$ (Tot.) (dex)
Li I	−9.47	0.05	0.06	−0.01	0.00	0.06	0.08
C I	−3.45	0.08	−0.05	0.05	0.00	0.07	0.11
N I	−3.95		−0.06	0.05	0.00	0.08	0.11
O I	−3.10		−0.08	0.05	0.00	0.09	0.12
Na I	−5.63	0.04	0.04	−0.04	−0.02	0.06	0.07
Mg I	−4.30	0.13	0.04	−0.02	−0.02	0.05	0.14
Mg II	−4.29	0.05	−0.08	0.04	−0.02	0.09	0.10
Al I	−5.63	0.08	0.03	−0.01	−0.01	0.03	0.09
Si I	−4.47	0.18	0.02	−0.01	−0.01	0.02	0.18
Si II	−4.33	0.01	−0.07	0.06	−0.02	0.09	0.09
S I	−4.78	0.05	0.06	−0.06	0.00	0.08	0.10
K I	−6.12		0.08	−0.08	−0.04	0.12	0.14
Ca I	−5.48	0.07	0.07	−0.05	−0.06	0.10	0.13
Ca II	−5.41	0.06	−0.06	0.04	−0.02	0.07	0.10
Sc II	−8.55	0.07	0.01	0.07	−0.04	0.08	0.11
Ti I	−6.95	0.09	0.08	0.00	−0.02	0.08	0.12
Ti II	−6.76	0.09	0.00	0.07	−0.06	0.09	0.13
V I	−7.99	0.07	0.09	0.00	−0.01	0.09	0.11
V II	−7.86	0.03	0.00	0.08	−0.01	0.08	0.09
Cr I	−6.17	0.06	0.06	−0.01	−0.02	0.06	0.09
Cr II	−5.94	0.06	−0.02	0.08	−0.03	0.09	0.11
Mn I	−6.41	0.16	0.07	0.00	−0.03	0.08	0.18
Fe I	−4.31	0.12	0.06	−0.02	−0.04	0.07	0.14
Fe II	−4.22	0.06	−0.02	0.07	−0.04	0.08	0.10
Co I	−6.98	0.07	0.07	0.00	−0.01	0.07	0.10
Ni I	−5.64	0.10	0.06	−0.01	−0.03	0.07	0.12
Cu I	−7.81	0.09	0.06	0.00	−0.02	0.06	0.11
Zn I	−7.32		0.02	0.02	−0.02	0.03	0.09
Sr I	−8.30		0.02	−0.01	−0.03	0.04	0.09
Sr II	−8.35	0.05	0.00	0.02	−0.02	0.03	0.06
Y II	−9.55	0.09	0.01	0.08	−0.03	0.09	0.12
Zr II	−9.08		0.01	0.08	−0.01	0.08	0.11
Ba II	−9.37	0.06	0.04	0.02	−0.11	0.12	0.13
La II	−10.40		0.03	0.08	−0.01	0.09	0.12
Ce II	−10.29	0.07	0.03	0.08	−0.01	0.09	0.11
Nd II	−10.45	0.03	0.03	0.08	−0.01	0.09	0.09
Sm II	−10.64		0.02	0.08	−0.02	0.08	0.12
Eu II	−11.30		0.03	0.08	−0.01	0.09	0.12
Gd II	$\leqslant -10.92$		0.02	0.08	0.00	0.08	0.11

Notes. The third column shows the standard deviation $\sigma_{\rm abn}$ (scatt.) of the mean abundance obtained from different spectral lines (internal scattering); a blank means that only a single line was used, and we estimated the internal scattering to be 0.08 dex. Note that these values are identical to those given in Table 2. Columns 4–6 give the variation in abundance estimated by increasing $T_{\rm eff}$ by 100 K, $\log g$ by 0.2 dex, and $\upsilon_{\rm mic}$ by 0.3 km s^{-1}, respectively. Column 7 gives the mean error bar calculated adding the systematic uncertainties given in Columns 4–6 in quadrature, i.e., $\sigma^2_{\rm abn}$ (syst.) $= \sigma^2_{\rm abn}$ ($T_{\rm eff}$) $+ \sigma^2_{\rm abn}$ ($\log g$) $+ \sigma^2_{\rm abn}$ ($\upsilon_{\rm mic}$). Column 8 gives the total mean error bar: $\sigma^2_{\rm abn}$ (tot.) $= \sigma^2_{\rm abn}$ (syst.) $+ \sigma^2_{\rm abn}$ (scatt.).

a simultaneous Markov chain Monte Carlo (MCMC) fit to radial velocity and transit light curve measurements produced values for $R_{\rm P}/R_*$, R_*, M_*, and the orbital semi-major axis a. The observed spectral type of the star and its radius imply the luminosity and the spectral energy distribution. Using this information, the Two Micron All Sky Survey (2MASS) IR fluxes can be used to derive the distance (IRFM; Blackwell et al. 1979). This method yields a distance to WASP-12 of 265 ± 20 pc (http://www.superwasp.org/wasp_planets.htm), assuming a typical main-sequence stellar radius; and 385 ± 30 pc, assuming the stellar radius from the MCMC fits of Hebb et al. (2009) (B. Smalley 2010, private communication). We note that the IRFM implicitly assumes solar metallicity and zero reddening, both inapplicable for WASP-12. Since the orbital period and the radial velocity amplitude fix the value of a, and the transit light curve fixes the ratio a:R_*, the stellar distance of 385 ± 30 pc is to be preferred. Hebb et al. (2009) also estimated the age of WASP-12 by fitting isochrones to the position of WASP-12 in a modified H-R diagram (temperature versus inverse cube root of the stellar density), obtaining an age of $2.0^{+0.5}_{-0.8}$ Gyr old; given the several uncertainties, they increased the error bars to 1 Gyr, concluding that WASP-12 is 2 ± 1 Gyr old.

One of the most secure empirical properties of the star is its color, or equivalently effective temperature. We can assess the distance and age of WASP-12 by comparing the effective temperature with isochrones and evolutionary tracks. Figure 7 shows four isochrones from Marigo et al. (2008)

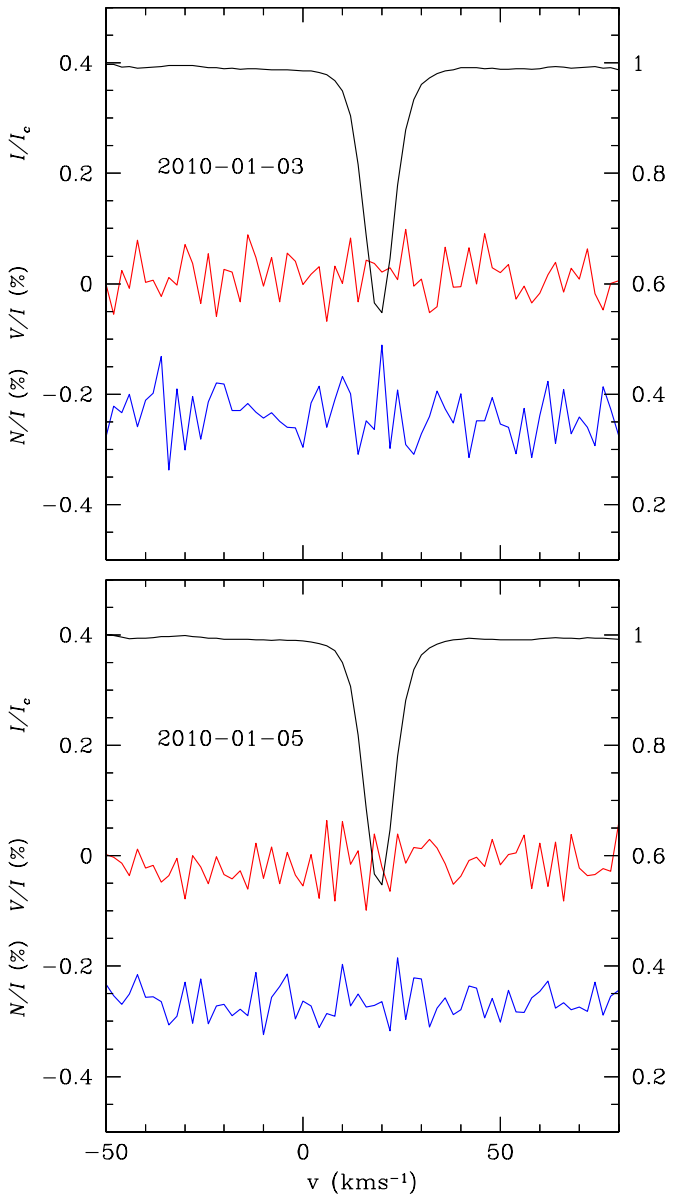

Figure 5. LSD profiles from the spectra obtained on January 3rd (top panel), corresponding to an orbital phase of 0.80, and 2010 January 5th (bottom panel), corresponding to an orbital phase of 0.81. In each panel, the top black line shows Stokes *I*, normalized to the continuum (the corresponding units are given in the right *y*-axis). The middle red line corresponds to the V/I profile and the bottom blue line to the null profile (Donati et al. 1997); their corresponding units are given in the left *y*-axis. The Stokes *I* LSD profile is centered on the stellar radial velocity and the null profile is shifted downward by an arbitrary offset.

(A color version of this figure is available in the online journal.)

with a metallicity Z of 0.030, the maximum available value of Z, adopted following Equation (2). WASP-12's effective temperature places it on the vertical thick blue line of Figure 7, where the other two full vertical blue lines are defined by the uncertainty on $T_{\rm eff}$. On this central line we placed three points, which correspond to distances of 265 pc (lower point), 295 pc (middle point), and 465 pc (upper point). The lower point lies well below the zero-age main sequence (ZAMS). From this we can rule out a distance as close as 265 pc; this concurs with the MCMC fitting of Hebb et al. (2009) in implying the star is bigger than the typical main-sequence stellar radius.

We can see that a range of possible ages and distances are compatible with the isochrones. In the region of Figure 7 between the two solid triangles, several isochrones are consistent with the empirical effective temperature. The 2.65 Gyr isochrone is just consistent with the lower limit on WASP-12's effective temperature: the loop to the right at the main-sequence turn-off point of this isochrone intersects the lower limit on the temperature. No star of this age is consistent with WASP-12's color except for those which are turning on to the horizontal branch, higher up in the diagram at $\log L/L_{\odot} \approx 1$. For stars at this stage of evolution $\log g \approx 3.8$, whereas the spectrum of WASP-12 implies $\log g \approx 4.2$ (cf. Section 4). WASP-12 thus cannot be turning on to the horizontal branch. Consequently we can constrain the position of WASP-12 in Figure 7 to be around or younger than the main-sequence turn-off.

Applying this reasoning, the oldest possible age for WASP-12 is 2.65 Gyr. This arises from the intersection of lower limit on WASP-12's effective temperature and the full thick isochrone in Figure 7. For all isochrones younger than this, there is also an intersection at or before the main-sequence turn-off. For the isochrones older than this no allowed intersection occurs: only evolved stars have compatible temperatures, but these are ruled out by their surface gravity.

The full red lines in Figure 7 are evolutionary tracks, from Girardi et al. (2000), for stars of mass 1.2 $M/M_{\odot}$, 1.3 $M/M_{\odot}$, 1.4 $M/M_{\odot}$, and 1.5 $M/M_{\odot}$, respectively, from bottom to top. WASP-12 is clearly hotter than a 1.2 $M/M_{\odot}$ star for any age, therefore we conclude its mass exceeds 1.2 $M/M_{\odot}$. Interpolating between the evolutionary tracks, we estimate a limit on the mass of WASP-12 of around 1.23 $M/M_{\odot}$. This is consistent with MCMC fitting of Hebb et al. (2009), but is a tighter constraint.

The evolutionary track for 1.3 $M/M_{\odot}$ almost exactly coincides with the intersection of the 2.65 Gyr isochrone with the lower limit on the effective temperature. The oldest possible age therefore corresponds to a stellar mass of about 1.3 $M/M_{\odot}$. For higher masses, the empirical effective temperature intersects the evolutionary track while the star is still on the main sequence and is therefore consistent with WASP-12's $\log g$. The 1.4 $M/M_{\odot}$ evolutionary track is consistent with the empirical effective temperature and is also consistent with the MCMC fitting of Hebb et al. (2009).

The upper limit on the mass from Hebb et al. (2009) is just below 1.5 $M/M_{\odot}$. We can use this to infer an upper limit on the luminosity, and hence the distance. We find that the maximum distance is 465 pc. On the other hand, the minimum distance is obtained at the intersection of the vertical line that defines WASP-12's effective temperature and the ZAMS; this distance is 295 pc. These distances are computed taking into account interstellar reddenings as given by Amôres & Lépine (2005).

One effective way to measure the age of a late-type star is the comparison of the lithium abundance with that of open cluster member stars for which the age is precisely known. For a more thorough analysis of the Li I line at 6707 Å we downloaded from the SOPHIE archive[14] all the 21 mid-resolution spectra[15] ($R \sim$ 40,000) of WASP-12 obtained for the radial velocity analysis published by Hebb et al. (2009).

Figure 8 shows a comparison between the 21 SOPHIE spectra and synthetic spectra calculated with the adopted stellar parameters and abundances around the region of the Li I line

[14] http://atlas.obs-hp.fr/sophie/

[15] SOPHIE is a cross-dispersed échelle spectrograph mounted at the 1.93 m telescope at the Observatoire de Haute-Provence (OHP).

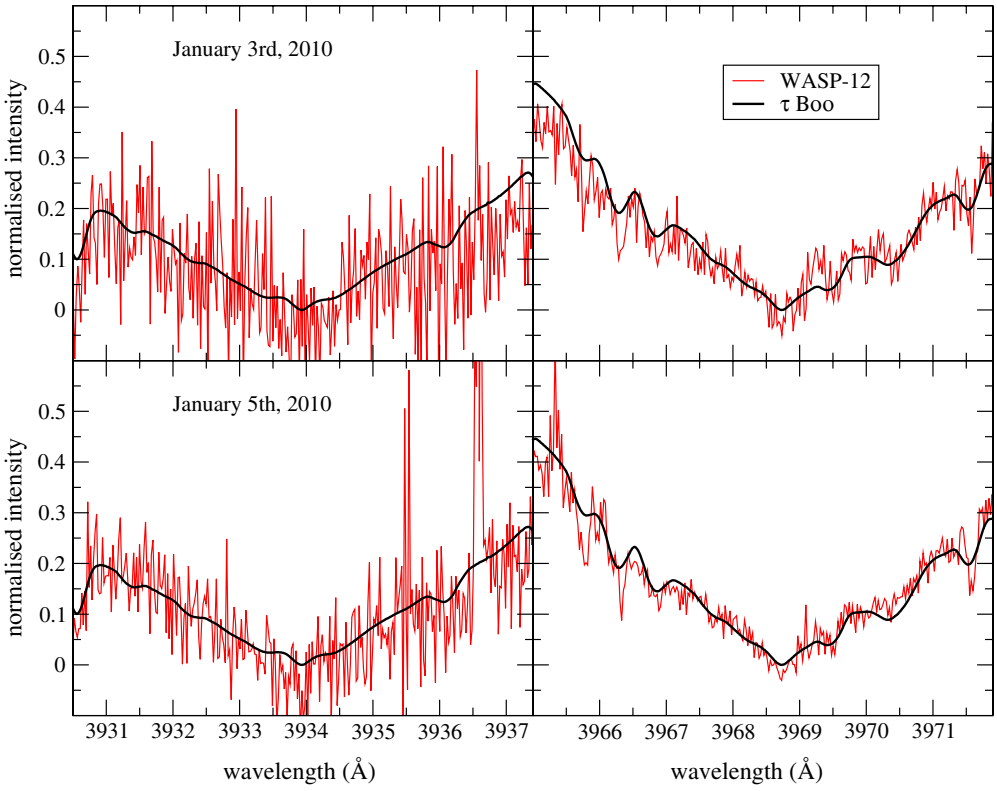

Figure 6. Comparison of the observed Ca K and H line (left and right panels, respectively) profiles between WASP-12 (thin line) and the planet-hosting star τ Boo (thick line; Shkolnik et al. 2005). The two upper panels show the WASP-12 spectrum obtained on 2010 January 3, while the two lower panels show the spectrum obtained on 2010 January 5.

(A color version of this figure is available in the online journal.)

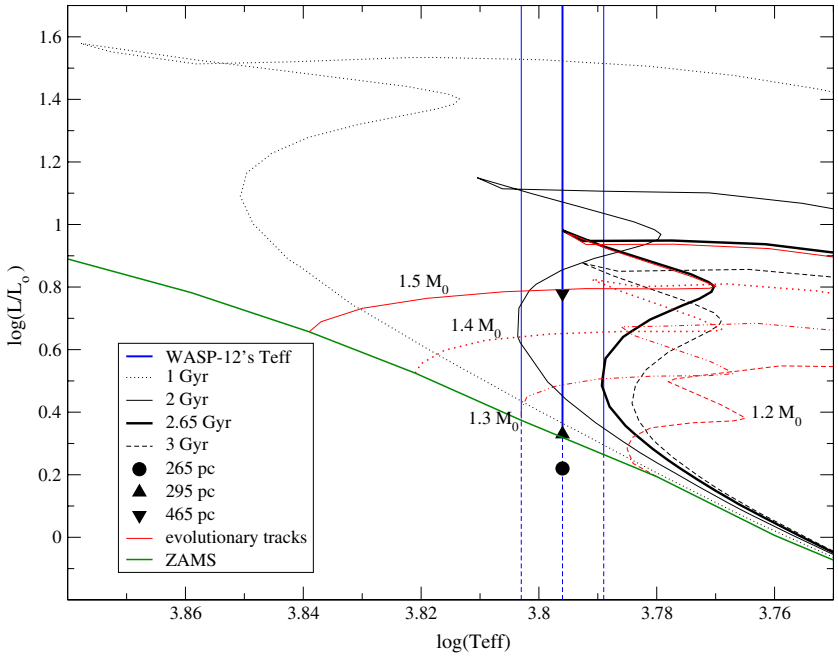

Figure 7. Position of WASP-12 on the H-R diagram assuming three different stellar distances: 265 pc (circle), 295 pc (triangle), and 465 pc (inverted triangle). The maximum and minimum distances were calculated adopting $T_{\rm eff} = 6250$ K and interstellar reddenings from Amôres & Lépine (2005). The dotted, thin full, and dashed lines show isochrones from Marigo et al. (2008) corresponding to ages of 1 Gyr, 2 Gyr, and 3 Gyr, respectively, encompassing the possible age range of WASP-12 from Hebb et al. (2009). The thick full line is the 2.65 Gyr isochrone we argue this is the maximum possible age for WASP-12. The red lines show evolutionary tracks from Girardi et al. (2000) for 1.5 $M/M_{\odot}$, 1.4 $M/M_{\odot}$, 1.3 $M/M_{\odot}$, and 1.2 $M/M_{\odot}$, from top to bottom. Both isochrones and evolutionary tracks assume a metallicity Z of 0.03. The blue vertical lines show the WASP-12's temperature range; these lines change from full to dashed below the ZAMS, indicated by the green line.

(A color version of this figure is available in the online journal.)

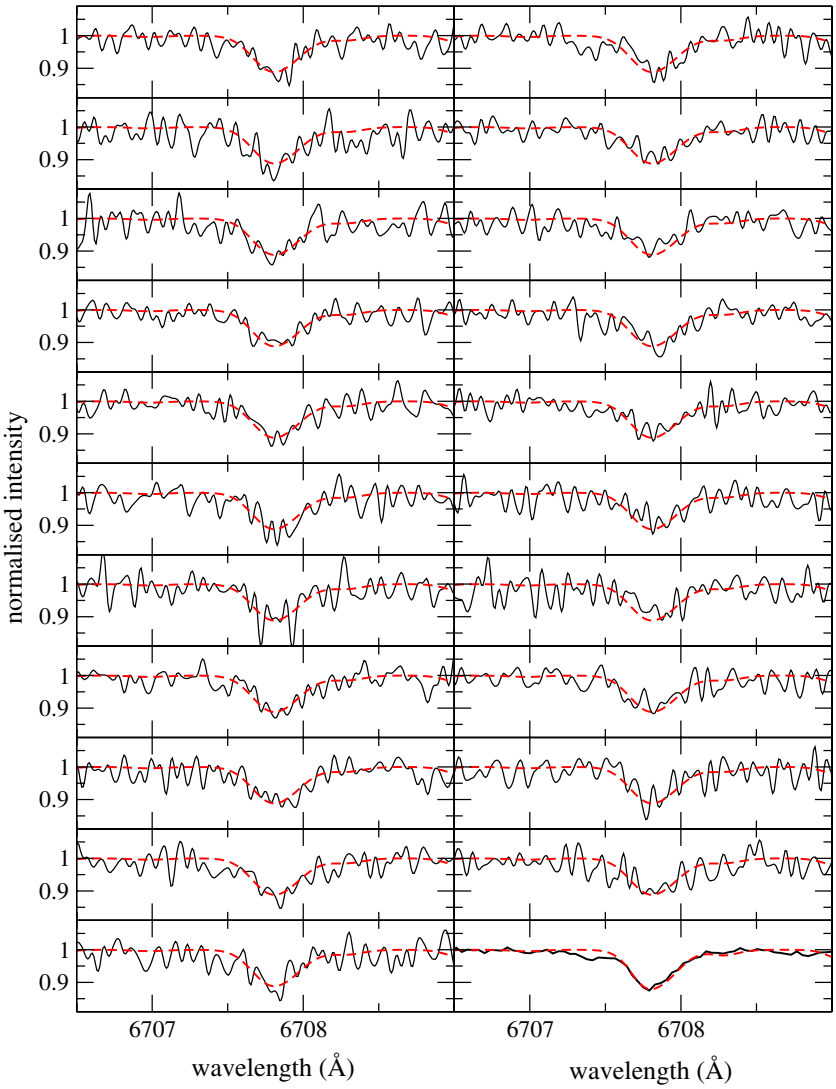

Figure 8. Comparison between the observed phase dependent SOPHIE spectra (black solid line) of WASP-12 around the Li I line at 6707 Å and synthetic spectra (dashed red line) calculated with the Li abundance and the parameters obtained from the analysis of the ESPaDOnS data. The bottom right panel shows the same comparison, but with the analyzed ESPaDOnS spectrum instead. The synthetic spectra take into account the difference in resolution between SOPHIE and ESPaDOnS.
(A color version of this figure is available in the online journal.)

at 6707 Å; the bottom right panel shows the same comparison, but with the ESPaDOnS spectrum. This plot shows that the Li abundance derived from the ESPaDOnS spectrum fits the SOPHIE data as well and that there is no line profile variation of the Li line with the orbital phase. We measured also the equivalent width of the Li line in each of these spectra and we did not find any significant time variation. For this reason, we believe that the lack of detection of this Li I line in the SARG spectrum of WASP-12, reported by Hebb et al. (2009), could be due to the low S/N or to a wrong line identification.

From a comparison between the lithium abundance of WASP-12 and the results published by Sestito & Randich (2005), we can only conclude that WASP-12 is older than 500 Myr, which is in agreement with the 2.0 ± 1.0 Gyr given by evolutionary tracks (Hebb et al. 2009). The large uncertainty is caused by the extremely slow lithium depletion for stars with effective temperatures similar to that of WASP-12, due to the shallow surface convection zone.

In conclusion, our analysis on the age of WASP-12 leads to a stellar age between 1.0 Gyr (lower limit given by Hebb et al. 2009) and 2.65 Gyr (from the analysis of the H-R diagram), as shown also in Table 4 that lists the minimum and maximum values we obtained for the stellar age, mass, and distance.

Table 4
Minimum and Maximum Values of WASP-12's Age (in Gyr), $M/M_{\odot}$ and Distance (in pc) as Derived by the Analysis of the H-R Diagram

Parameter	Minimum Value	Maximum Value
Age (Gyr)	1.0*	2.65
$M/M_{\odot}$	1.23	1.49*
Distance (pc)	295	465

Note. The values marked with an "*" are taken from Hebb et al. (2009).

6.3. Is WASP-12 a Chemically Peculiar Star?

One of the main purpose of this work is to search for chemical peculiarities that could be connected with pollution of the

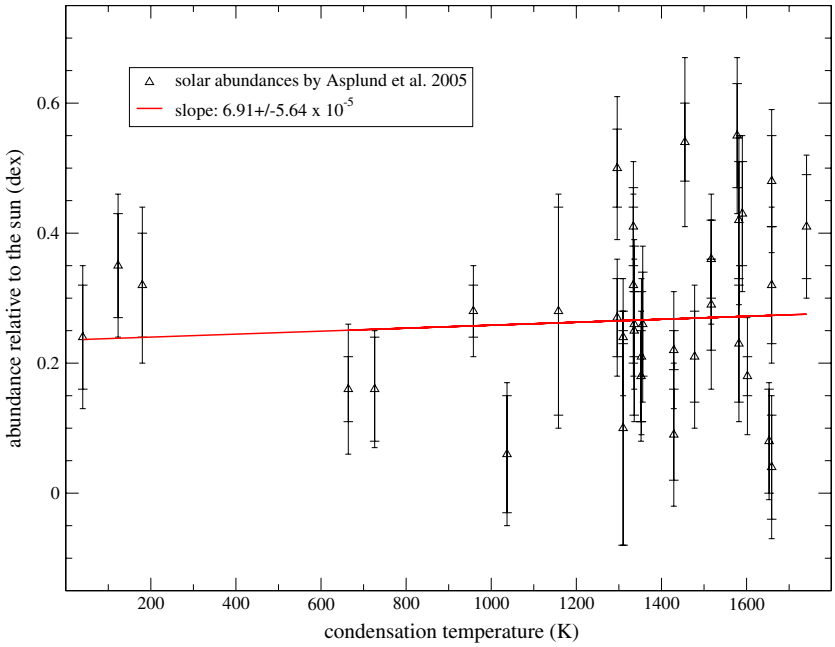

Figure 9. Ion abundance relative to the Sun (Asplund et al. 2005) as a function of the condensation temperature. The full line shows the linear fit to the data. The abundance uncertainties are given as in Figure 4.

(A color version of this figure is available in the online journal.)

stellar atmosphere by material lost by the planet. This can be done in different ways, as also shown in the extensive salient literature present (see, e.g., Neves et al. 2009, and references therein). WASP-12 is a promising target for signs of atmospheric pollution: WASP-12 b is most likely currently losing material (Fossati et al. 2010); this material is believed to be forming a circumstellar disk that is accreting onto the star, polluting the stellar photosphere (Li et al. 2010). Classical ways of looking for atmospheric pollution are by searching: (1) chemical peculiarities of single elements, such as Li and Be (e.g., Israelian et al. 2004); (2) a trend in the element abundance against the condensation temperature (T_c; see, e.g., Sadakane et al. 2002; Ecuvillon et al. 2006; Meléndez et al. 2009); (3) chemical peculiarities of the abundance pattern in comparison to reference stars (both planet-hosting and non-planet-hosting).

When searching for small effects on the stellar atmospheric abundances it is important to determine whether a certain star belongs to the thin or thick Galactic disk population. To do so we performed both a kinematic and chemical analysis of WASP-12. We calculated the Galactic velocity vectors (U, V, W) corrected to the local standard of rest using the formalism of Johnson & Soderblom (1987), instead defining U as positive toward the Galactic anti-center. As done by Sozzetti et al. (2006), WASP-12 was then placed on the Toomre diagram of the Soubiran & Girard (2005) stellar sample, indicating that WASP-12 has a peculiar velocity less than 85 km s^{-1}, strongly indicative of thin disk membership. From the WASP-12 abundances, we then compared our values of [α/Fe] (-0.15 dex) and [Fe/H] (+0.28 dex), where [α/Fe] is defined as 0.25([Mg/Fe]+[Si/Fe]+[Ca/Fe]+[Ti/Fe]), with the Soubiran & Girard (2005) sample, obtaining that WASP-12 is again consistent with the properties of the thin disk population.

In our analysis, we are not able to look for chemical peculiarities of both Li and Be. As shown in Figure 8, our spectra do not have the S/N and the resolution necessary to perform a precise analysis of the Li^6/Li^7 ratio, but we can compare the lithium abundance obtained for WASP-12 with that of other planet-hosting stars. Israelian et al. (2004) and Gonzalez et al. (2010a) published lithium abundances of stars hosting a giant planet or a brown dwarf and compared them to a set of non-planet-hosting stars. The lithium abundance we obtained for WASP-12 matches that of both set of stars, showing clearly that Li is not peculiar in WASP-12. Our spectra do not include the region around 3130 Å covering the two Be II lines usually adopted to measure the Be abundance.

6.3.1. Volatile Versus Refractory Elements

An effective way to check whether a stellar photosphere is polluted by accretion of metal-rich material is to examine the correlation between the relative abundance of various elements and their T_c. In accreting metal-rich material the refractory elements tend to form dust grains that are blown away by the stellar wind. Thus, the star accretes more volatile than refractory elements, as happens, for example, in λ Bootis stars (Martínez-Galarza et al. 2009). Our WASP-12 ion abundance is shown against condensation temperature (taken from Lodders 2003) in Figure 9.

The correlation obtained between the ion abundances relative to the Sun (Asplund et al. 2005) and T_c is not statistically significant: $6.91 \pm 5.64 \times 10^{-5}$. In the past years several authors (e.g., Sadakane et al. 2002; Ecuvillon et al. 2006; Sozzetti et al. 2006) looked for the same kind of correlation in several planet-hosting stars, without having found any. The trend we obtain for WASP-12 is also indicative of a null result.

Meléndez et al. (2009), applying a differential analysis on the Sun and solar twins, discovered that the Sun shows a highly significant correlation of the abundances (relative to the mean abundance of the solar twins) in respect to the condensation temperature. In addition, this correlation shows a significant break at $T_c \sim 1200$ K. Meléndez et al. (2009)

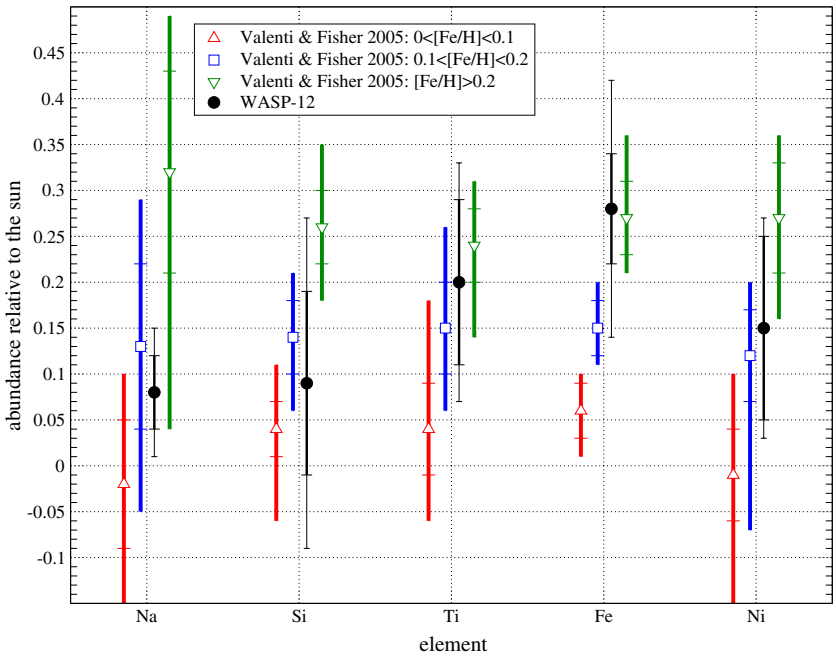

Figure 10. Comparison between the mean abundance, relative to the Sun, of WASP-12 (full circles) and of the selected sample of stars from Valenti & Fisher (2005), that was subdivided according to the iron abundance: $0.0 < [Fe/H] \leqslant 0.1$ dex (open upside triangles), $0.1 < [Fe/H] \leqslant 0.2$ dex (open squares), and $[Fe/H] > 0.2$ dex (open downside triangles). The shaded areas show the abundance range, while the error bars of the comparison sample give the standard deviation from the mean abundance. The uncertainties on the abundances of WASP-12 are as in Figure 4.

(A color version of this figure is available in the online journal.)

and Gonzalez et al. (2010b) came to the conclusion that this correlation is likely connected to the presence of planets around the Sun. The detection of this kind of correlation requires very high precision abundances (error bars < 0.05 dex and free from systematic differences), attainable only with a differential analysis. The application of this method to WASP-12 would require observations of stars that can be considered twins of WASP-12 (similar $T_{\rm eff}$, metallicity, age, and population). The choice of the WASP-12 twins will be of crucial importance because effects such as diffusion, more prevalent for F-type stars than G-type stars, are strongly age and $T_{\rm eff}$ dependent, and consequently could easily hide or mimic pollution signatures.

Our analysis does not lead to a firm conclusion about the atmospheric pollution of WASP-12.

6.3.2. Comparison with Previous Analysis

To check whether WASP-12 has a peculiar abundance pattern we compared the abundances with those obtained by other authors on a large number of stars with a similar $T_{\rm eff}$. In particular, we took into account the results of the abundance analysis on stars that are not known planet hosts, in the temperature range 6000–6500 K, and with an $[Fe/H] > 0.0$ dex. We decided to use such a small temperature range to decrease the effect of possible systematics, such as non-LTE effects. In addition, since we are interested in looking for a peculiar pattern, we decided to use only the stars with an oversolar iron abundance and to subdivide the sample of comparison stars according to their iron abundance: $0.0 < [Fe/H] \leqslant 0.1$, $0.1 < [Fe/H] \leqslant 0.2$, and $[Fe/H] > 0.2$. To have a better statistical view of each subsample we decided to plot in our comparisons not only the mean abundance and relative standard deviation for the comparison stars, but also their abundance range. To accomplish all these requirements, we needed to have a large set of non-planet-hosting stars, such as the one provided by Valenti & Fisher (2005).

Valenti & Fisher (2005) performed a parameter determination and LTE abundance analysis of more than 1000 late-type main sequence stars. For each star, they derived the abundances of Na, Si, Ti, Fe, and Ni. This sample provided us with comparison abundances for 59 stars with $0.0 < [Fe/H] \leqslant 0.1$ dex, 36 stars with $0.1 < [Fe/H] \leqslant 0.2$ dex, and 22 stars with $[Fe/H] > 0.2$ dex. The comparison between our WASP-12 abundances and the ones from the sample of Valenti & Fisher (2005) is shown in Figure 10.

Figure 10 shows that the abundances of Ti and Fe are clearly comparable to the ones of the higher metallicity subsample, as expected given the fact that [Fe/H] of WASP-12 is about 0.3. The Na abundance of WASP-12 falls within the abundance range of the high-metallicity stars of the comparison sample, due to the large range covered by the Na abundance, while Ni shows a mean abundance that is just outside the abundance range. The Si abundance looks definitely more similar to the one of the set of stars with $0.1 < [Fe/H] \leqslant 0.2$ dex, but the large uncertainty on this abundance does not allow any firm conclusion. In summary, the abundances of Ti and Fe follow the pattern of the high-metallicity stars, while Na, Si, and Ni seem to follow more the abundance pattern of the set of comparison stars with [Fe/H] between 0.1 and 0.2 dex.

The information gathered from this comparison leads to the conclusion that there is the possibility that the WASP-12 abundances of Na, Si, and Ni do not really match the abundance pattern that the WASP-12 iron abundance would suggest. But it has to be taken into account that the comparison is not free from systematic differences in the fundamental parameters and abundance determinations, and in the set of adopted atomic line parameters.

For a further search of possible abundance peculiarities in the atmosphere of WASP-12 we decided to compare our results with those of several other authors (Takeda et al. 2002; Sadakane et al. 2002; Ecuvillon et al. 2004; Sozzetti et al. 2006; Gilli et al.

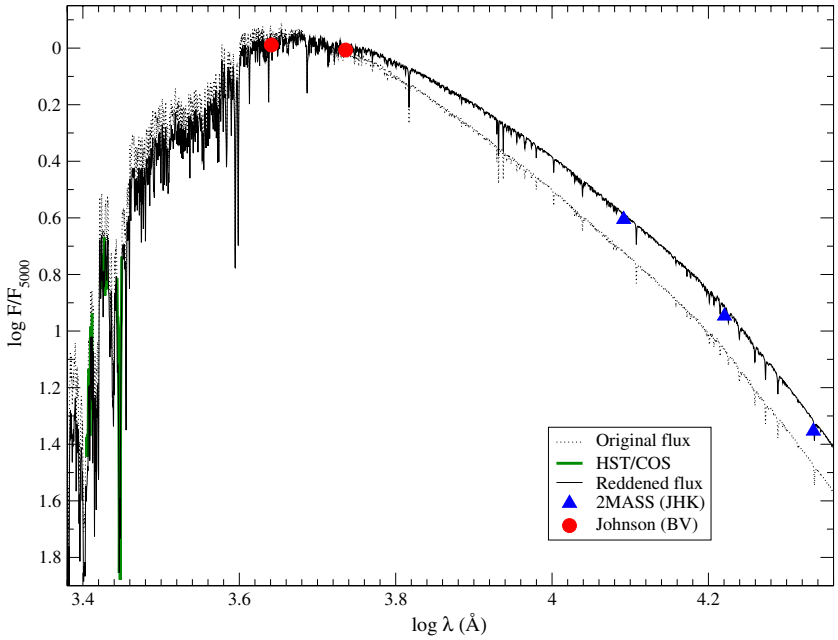

Figure 11. Comparison between LLMODELS theoretical fluxes calculated with the fundamental parameters and abundances derived for WASP-12, taking into account a reddening of $E(B-V) = 0.126$ mag (full line) and without taking into account reddening (dashed line), with COS calibrated fluxes (thick gray line), Johnson BV photometry (full points), and 2MASS photometry (full triangles). The error bars on the photometry have the same size of the symbols. The model fluxes and the COS spectra were convolved to have approximately a spectral resolution of 800, for display reasons.

(A color version of this figure is available in the online journal.)

2006; Santos et al. 2006; Bond et al. 2008; Neves et al. 2009) have obtained in planet-hosting and non-planet-hosting stars. In this way we should also be able to partially remove possible systematic differences in case a peculiar pattern becomes evident in the comparisons with several different authors.

The WASP-12 abundances we derived for O, Ca, Sc, Mn, Zn, Y, Zr, Nd, and Eu match very well the ones previously obtained by other authors in planet-hosting and non-planet-hosting stars, while abundances of Al, V, and Cu appear to be clearly below the values previously obtained by more than 0.2 dex. For the other compared elements (C, N, Na, Mg, Si, S, Ti, Cr, Co, and Ni) we obtained just a satisfactory agreement, since we register a tendency of the WASP-12 abundances of these elements to lay always in the lower margin of the comparison samples, in particular when the abundances are put in relation to the iron abundance. This result follows what previously obtained, strengthening the possibility of an increased Fe abundance in comparison to the one of some other elements.

In addition, we compared our Si, Ti, and Ni WASP-12 abundances with the ones obtained by Robinson et al. (2006) in a set of planet-hosting and non-planet-hosting stars. We obtained a good agreement for Ti, but both Si and Ni appear to be depleted in WASP-12, compared to the abundances obtained by Robinson et al. (2006) in a set of planet-hosting stars, therefore we cannot confirm their conclusion of a systematic enrichment of Si and Ni in planet-hosting compared to non-planet-hosting stars.

6.4. Spectral Energy Distribution: Searching for a Circumstellar Disk

The circumstellar disk, predicted by Li et al. (2010) and tentatively observed by Fossati et al. (2010), could be detectable in the infrared. For this reason, we decided to compare the calibrated near-UV COS fluxes of WASP-12 and the available photometry (Johnson and 2MASS photometry) with synthetic fluxes obtained with LLMODELS adopting the fundamental parameters and the abundances derived from the ESPaDOnS data, looking for an infrared excess in the 2MASS photometry. For this comparison, shown in Figure 11, we took into account a reddening $E(B-V) = 0.126$ mag (Amôres & Lépine 2005) that was calculated assuming the stellar distance obtained in Section 6.2.

Figure 11 shows a very good agreement between the model fluxes and the observations, demonstrating also the quality of both the adopted fundamental parameters and interstellar reddening.

Figure 11 does not show any clear infrared excess in the 2MASS photometry that could be interpreted as (1) there is no interstellar disk around the star or (2) the interstellar disk is not visible because either the emission is not strong enough or the emission peaks at much longer wavelengths. Li et al. (2010) suggested that the disk emission should peak at $\sim$2.3 μm, inside the wavelength range covered by the K-band 2MASS photometry. Therefore, to look for an interstellar disk around WASP-12 it would be necessary to observe the system with a very high precision (Li et al. 2010) and at longer wavelengths, both accessible with the Herschel satellite (Pilbratt et al. 2010).

7. CONCLUSIONS

On 2010 January 3 and 5, we observed the planet-hosting star WASP-12 with the ESPaDOnS spectropolarimeter with the aim of looking for a global magnetic field, derive the stellar parameters and perform a precise abundance analysis.

The WASP-12 fundamental parameters and iron abundance we obtained are in agreement with what previously published by Hebb et al. (2009): $T_{\rm eff} = 6250 \pm 100$ K, $\log g = 4.2 \pm 0.2$, $\upsilon_{\rm mic} = 1.2 \pm 0.3$ km s^{-1}, and [Fe/H] $= 0.32 \pm 0.12$ dex. $\upsilon \sin i$ is less than 4.6 ± 0.5 km s^{-1}, while $\upsilon_{\rm macro}$ lies within the range $4.75–7.0 \pm 0.6$ km s^{-1}. Dedicated observations to measure the amplitude of the RM effect are necessary to derive the real stellar $\upsilon \sin i$. The resultant metallicity of WASP-12 is $Z = 0.021 \pm$

0.002 dex. A detailed analysis of the H-R diagram, with the use of isochrones and evolutionary tracks allowed to derive more accurate ranges for the stellar age, mass, and distance: the age of WASP-12 is between 1.0 Gyr (Hebb et al. 2009) and 2.65 Gyr, the mass is between 1.23 and 1.49 $M/M_{\odot}$ (the last value comes from Hebb et al. 2009), and the distance to WASP-12 is between 295 and 465 pc. Our measurement of the Li abundance allowed us just to conclude that WASP-12 is older than 500 Myr.

We performed a magnetic field search adopting the LSD technique revealing that the star does not show any magnetic field signature in Stokes *V*. A detailed analysis of the possible star–planet magnetic interaction would require a time-dependent analysis of particular spectral lines, such as the Ca H and K lines (Shkolnik et al. 2003, 2005, 2008) and the Mg II UV resonance lines, but it has to be taken into account that WASP-12 shows a remarkably low stellar activity (Knutson et al. 2010), that will be analyzed in detail in a forthcoming paper.

Given recent theoretical predictions (Li et al. 2010) and discoveries (Fossati et al. 2010), the WASP-12 system seems to be an ideal target to detect the presence of atmospheric pollution, due to the material lost by the planet. Therefore, we looked for hints of pollution by looking for a correlation between the atmospheric element abundances and the condensation temperature, and by comparing the WASP-12 abundance pattern with the one of other planet-hosting and non-planet-hosting stars, previously published by several other authors. Our analysis revealed just the presence of hints of atmospheric pollution, although only a differential analysis would allow to obtain firm evidences. One must also take into account the fact that it is not clear whether WASP-12 would show the same kind of atmospheric pollution shown by the Sun (Meléndez et al. 2009): the material coming from WASP-12 b and falling onto the star is in a gas/plasma state and only a detailed modeling of the temperature and density structure of the accretion disk would show whether the material is condensing in dust grains. If dust grains are forming it is likely that a differential analysis would reveal the kind of pollution signatures obtained for the Sun, otherwise all the material lost by the planet would fall onto the star, making then the pollution signature dependent on the unknown hydrogen content of the planet.

With the use of the available *HST* calibrated spectra and of visible and infrared photometry, we looked for the presence of a circumstellar disk around WASP-12, but without success. Probably high precision far infrared measurements, such as those possible with the Hershel satellite, may reveal the presence of a circumstellar disk.

This work is based on observations obtained at the Canada–France–Hawaii Telescope (CFHT), which is operated by the National Research Council of Canada, the Institut National des Sciences de l'Univers of the Centre National de la Rechereche Scientifique of France, and the University of Hawaii. This work is also based on observations made with the NASA/ESA Hubble Space Telescope, obtained from MAST at the Space Telescope Science Institute, which is operated by the Association of Universities for Research in Astronomy, Inc., under NASA contract NAS 5-26555. These observations are associated with program 11651 to which support was provided by NASA through a grant from the Space Telescope Science Institute. This publication makes use of data products from the Two Micron All Sky Survey, which is a joint project of the University of Massachusetts and the Infrared Processing and Analysis Center/California Institute of Technology, funded by the National Aeronautics and Space Administration and the National Science Foundation. This work is supported by an STFC Rolling Grant (L.F., A.E.). O.K. is a Royal Swedish Academy of Sciences Research Fellow supported by grants from the Knut and Alice Wallenberg Foundation and the Swedish Research Council. D.S. acknowledges support received from the Deutsche Forschungsgemeinschaft (DFG) Research Grant RE1664/7-1. L.F. is deeply in debt with Dr. Tanya Ryabchikova for the tremendous help she gave with the log gf values' references, Dr. Gregg Wade for his help during the preparation of the observing proposal, and Dr. Berry Smalley for the information regarding the determination of the WASP-12 distance. We also thank the CFHT staff, Dr. Nadine Manset, and the CFHT director, Dr. Christian Veillet, for their help and speed in obtaining the observations.

Facilities: HST (COS), CFHT (ESPaDOnS), OHP:1.93m (SOPHIE).

REFERENCES

Aldenius, M., Tanner, J. D., Johansson, S., Lundberg, H., & Ryan, S. G. 2007, A&A, 461, 767
Amôres, E. B., & Lépine, J. R. D. 2005, AJ, 130, 659
Asplund, M., Grevesse, N., & Sauval, A. J. 2005, in ASP Conf. Ser. 336, Cosmic Abundances as Records of Stellar Evolution and Nucleosynthesis, ed. T. G. Barnes III & F. N. Bash (San Francisco, CA: ASP), 25
Bard, A., & Kock, M. 1994, A&A, 282, 1014
Bard, A., Kock, A., & Kock, M. 1991, A&A, 248, 315
Berry, H. G., Bromander, J., Curtis, L. J., & Buchta, R. 1971, Phys. Scr., 3, 125
Bielski, A. 1975, J. Quant. Spectrosc. Radiat. Transfer, 15, 463
Biemont, E., Quinet, P., & Zeippen, C. J. 1993, A&AS, 102, 435
Bizzarri, A., et al. 1993, A&A, 273, 707
Blackwell, D. E., Shallis, M. J., & Selby, M. J. 1979, MNRAS, 188, 847
Blanco, F., Botho, B., & Campos, J. 1995, Phys. Scr., 52, 628
Böhm-Vitense, E. 1958, Z. Astrophys., 46, 108
Bond, J. C., et al. 2008, ApJ, 682, 1234
Burrows, A., Hubeny, I., Budaj, J., & Hubbard, W. B. 2007, ApJ, 661, 502
Canuto, V. M., & Mazzitelli, I. 1991, ApJ, 370, 295
Canuto, V. M., & Mazzitelli, I. 1992, ApJ, 389, 724
Cowley, C. R., & Bord, D. J. 1998, in ASP Conf. Ser. 143, The Scientific Impact of the Goddard High Resolution Spectrograph, ed. J. C. Brandt, T. B. Ake, & C. C. Petersen (San Francisco, CA: ASP), 346
Cowley, C. R., & Corliss, C. H. 1983, MNRAS, 203, 651
Den Hartog, E. A., Lawler, J. E., Sneden, C., & Cowan, J. J. 2003, ApJS, 148, 543
Donati, J.-F., Semel, M., Carter, B. D., Rees, D. E., & Collier Cameron, A. 1997, MNRAS, 291, 658
Donati, J.-F., et al. 2007, MNRAS, 380, 1297
Ecuvillon, A., Israelian, G., Santos, N. C., Mayor, M., & Gilli, G. 2006, A&A, 449, 809
Ecuvillon, A., Israelian, G., Santos, N. C., Mayor, M., Villar, V., & Bihain, G. 2004, A&A, 426, 619
Fares, R., et al. 2010, MNRAS, 406, 409
Fossati, L., Ryabchikova, T., Bagnulo, S., Alecian, E., Grunhut, J., Kochukhov, O., & Wade, G. 2009, A&A, 503, 945
Fossati, L., et al. 2010, ApJ, 714, L222
Fuhr, J. R., Martin, G. A., & Wiese, W. L. 1988, J. Phys. Chem. Ref. Data, 17, Suppl. 4
Fuhrmann, K., Pfeiffer, M., Frank, C., Reetz, J., & Gehren, T. 1997, A&A, 323, 909
Gilli, G., Israelian, G., Ecuvillon, A., Santos, N. C., & Mayor, M. 2006, A&A, 449, 723
Girardi, L., Bressan, A., Bertelli, G., & Chiosi, C. 2000, A&AS, 141, 371
Gonzalez, G., Carlson, M. K., & Tobin, R. W. 2010a, MNRAS, 403, 1368
Gonzalez, G., Carlson, M. K., & Tobin, R. W. 2010b, MNRAS, in press (arXiv:1004.3313)
Green, J. C., et al. 2010, BAAS, 41, 501
Guillot, T. 2005, Annu. Rev. Earth Planet. Sci., 33, 493
Hannaford, P., Lowe, R. M., Grevesse, N., Biemont, E., & Whaling, W. 1982, ApJ, 261, 736
Hebb, L., et al. 2009, ApJ, 693, 1920
Heiter, U., et al. 2002, A&A, 392, 619
Husnoo, N., et al. 2010, MNRAS, submitted (arXiv:1004.1809)

Israelian, G., Santos, N. C., Mayor, M., & Rebolo, R. 2004, A&A, 414, 601
Johnson, D. R. H., & Soderblom, D. R. 1987, AJ, 93, 864
Knutson, H. A., Howard, A. W., & Isaacson, H. 2010, ApJ, submitted (arXiv:1004.2702)
Kochukhov, O. 2007, in Proc. Int. Conf., Physics of Magnetic Stars, 109, ed. I. Romanyuk & D. O. Kudryavtsev (Zelenchukskiy: Special Astrophysical Observatory of the Russian AS), 118
Kupka, F., Piskunov, N., Ryabchikova, T. A., Stempels, H. C., & Weiss, W. W. 1999, A&AS, 138, 119
Kurucz, R. 1993a, ATLAS9: Stellar Atmosphere Programs and 2 km/s Grid, Kurucz CD-ROM No. 13 (Cambridge, MA: Smithsonian Astrophysical Observatory)
Kurucz, R. L. 1993b, CDROM 20-22 (Cambridge MA: Smithsonian Astrophysical Observatory)
Kurucz, R. L. 1988, in Trans. IAU, XXB, Transactions of the International Astronomical Union, ed. M. McNally (Dordrecht: Kluwer), 168
Kurucz, R. L., & Peytremann, E. 1975, SAO Special Report, 362
Lai, D., Helling, C., & van den Heuvel, E. P. J. 2010, ApJ, submitted (arXiv:1005.4497)
Lambert, D. L., Mallia, E. A., & Warner, B. 1969, MNRAS, 142, 71
Lawler, J. E., Bonvallet, G., & Sneden, C. 2001a, ApJ, 556, 452
Lawler, J. E., & Dakin, J. T. 1989, J. Opt. Soc. Am. B: Opt. Phys, B6, 1457
Lawler, J. E., Den Hartog, E. A., Sneden, C., & Cowan, J. J. 2006, ApJS, 162, 227
Lawler, J. E., Sneden, C., Cowan, J. J., Ivans, I. I., & Den Hartog, E. A. 2009, ApJS, 182, 51
Lawler, J. E., Wickliffe, M. E., Den Hartog, E. A., & Sneden, C. 2001b, ApJ, 563, 1075
Li, S., Miller, N., Lin, D. N. C., & Fortney, J. J. 2010, Nature, 463, 1054
Lincke, R., & Ziegenbein, G. 1971, Z. Phyzik, 241, 369
Ljung, G., Nilsson, H., Asplund, M., & Johansson, S. 2006, A&A, 456, 1181
Lodders, K. 2003, ApJ, 591, 1220
Marigo, P., Girardi, L., Bressan, A., Groenewegen, M. A. T., Silva, L., & Granato, G. L. 2008, A&A, 482, 883
Martin, G. A., Fuhr, J. R., & Wiese, W. L. 1988, J. Phys. Chem. Ref. Data, 17, Suppl. 3
Martínez-Galarza, J. R., Kamp, I., Su, K. Y. L., Gáspár, A., Rieke, G., & Mamajek, E. E. 2009, ApJ, 694, 165
Mashonkina, L. I. 2009, Phys. Scr. T, 134, 014004
Mashonkina, L., & Zhao, G. 2006, A&A, 456, 313
Mashonkina, L. I., Vinogradova, A. B., Ptitsyn, D. A., Khokhlova, V. S., & Chernetsova, T. A. 2007, Astron. Rep., 51, 903
Meléndez, J., Asplund, M., Gustafsson, B., & Yong, D. 2009, ApJ, 704, L66
Miles, B. M., & Wiese, W. L. 1969, WSG Technical Note 474
Neves, V., Santos, N. C., Sousa, S. G., Correia, A. C. M., & Israelian, G. 2009, A&A, 497, 563
Nitz, D. E., Wickliffe, M. E., & Lawler, J. E. 1998, ApJS, 117, 313
O'Brian, T. R., Wickliffe, M. E., Lawler, J. E., Whaling, W., & Brault, J. W. 1991, J. Opt. Soc. Am. B: Opt. Phys, B8, 1185
Osterman, S., et al. 2010, BAAS, 41, 502
Pickering, J. C., Thorne, A. P., & Perez, R. 2001, ApJS, 132, 403
Pilbratt, G. L., et al. 2010, A&A, 518, L1
Piskunov, N. E., Kupka, F., Ryabchikova, T. A., Weiss, W. W., & Jeffery, C. S. 1995, A&AS, 112, 525
Raassen, A.J.J., & Uylings, P.H.M. 1998, A&A, 340, 300 (ftp://ftp.wins.uva.nl/pub/orth)
Ralchenko, Yu., Kramida, A. E., Reader, J., & NIST ASD Team. 2008, NIST Atomic Spectra Database (version 3.1.5) (Gaithersburg, MD: NIST) (http://physics.nist.gov/asd3)
Robinson, S. E., Laughlin, G., Bodenheimer, P., & Fischer, D. 2006, ApJ, 643, 484
Ryabchikova, T. A., Fossati, L., & Shulyak, D. 2009, A&A, 506, 203
Ryabchikova, T. A., Piskunov, N. E., Stempels, H. C., Kupka, F., & Weiss, W. W. 1999, Phys. Scr., T83, 162
Sadakane, K., Ohkubo, M., Takeda, Y., Sato, B., Kambe, E., & Aoki, W. 2002, PASJ, 54, 911
Santos, N. C., et al. 2006, A&A, 458, 997
Seager, S., Whitney, B. A., & Sasselov, D. D. 2000, ApJ, 540, 504
Seaton, M. J., Mihalas, D., & Pradhan, A. K. 1994, MNRAS, 266, 805
Sestito, P., & Randich, S. 2005, A&A, 442, 615
Shkolnik, E., Bohlender, D. A., Walker, G. A. H., & Collier Cameron, A. 2008, ApJ, 676, 628
Shkolnik, E., Walker, G. A. H., & Bohlender, D. A. 2003, ApJ, 597, 1092
Shkolnik, E., Walker, G. A. H., Bohlender, D. A., Gu, P.-G., & Kürster, M. 2005, ApJ, 622, 1075
Shulyak, D., Tsymbal, V., Ryabchikova, T., Stütz, Ch., & Weiss, W. W. 2004, A&A, 428, 993
Smith, G. 1988, J. Phys. B: At. Mol. Opt. Phys., 21, 2827
Smith, G., & O'Neil, J. A. 1975, A&A, 38, 1
Smith, G., & Raggett, D. St. J. 1981, J. Phys. B: At. Mol. Phys., 14, 4015
Smith, V. V., Lambert, D. L., & Nissen, P. E. 1998, ApJ, 506, 405
Soubiran, C., & Girard, P. 2005, A&A, 438, 139
Southworth, J. 2009, MNRAS, 394, 272
Sozzetti, A., Yong, D., Carney, B. W., Laird, J. B., Latham, D. W., & Torres, G. 2006, AJ, 131, 2274
Takeda, Y., Kato, K.-I., Watanabe, Y., & Sadakane, K. 1996, PASJ, 48, 511
Takeda, Y., et al. 2002, PASJ, 53, 1211
Tsymbal, V. V. 1996, in ASP Conf. Ser. 108, Model Atmospheres and Spectral Synthesis, ed. S. J. Adelman, F. Kupka, & W. W. Weiss (San Francisco, CA: ASP), 198
Valenti, J. A., & Fisher, D. A. 2005, ApJS, 159, 141
Wade, G. A., Donati, J.-F., Landstreet, J. D., & Shorlin, S. L. S. 2000, MNRAS, 313, 823
Warner, B. 1968, MNRAS, 139, 115
Wickliffe, M. E., & Lawler, J. E. 1997, ApJS, 110, 163
Wiese, W. L., Fuhr, J. R., & Deters, T. M. 1996, A Critical Data Compilation, J. Phys. Chem. Ref. Data (Monograph No. 7; Melville, NY: AIP), 532
Wiese, W. L., Smith, M. W., & Miles, B. M. 1969a, NSRDS-NBS, 22
Wiese, W. L., Smith, M. W., & Miles, B. M. 1969b, NSRDS-WSG, 22
Zhao, G., & Gehren, T. 2000, A&A, 362, 1077